This is a preprint, the final version is subject to change, of the American Mineralogist (MSA)
Cite as Authors (Year) Title. American Mineralogist, in press.
(DOI will not work until issue is live.) DOI: http://dx.doi.org/10.2138/am-2016-5753

REVISION 1

Chemical zoning and lattice distortion in radiogenically modified minerals: uraninite from Olympic Dam Cu-U-Au-Ag deposit, South Australia

Edeltraud Macmillan[1,2], Cristiana L. Ciobanu[3], Kathy Ehrig[2], Nigel J. Cook[3], and Allan Pring[4]

[1]*School of Physical Sciences, The University of Adelaide, Adelaide, SA, 5005, Australia*

[2]*BHP Billiton Olympic Dam, Adelaide, SA, 5000, Australia*

[3]*School of Chemical Engineering, The University of Adelaide, Adelaide, SA, 5005, Australia*

[4]*School of Chemical and Physical Sciences, Flinders University, Bedford Park, SA, 5042, Australia*

ABSTRACT

Compositionally-zoned uraninite from the Olympic Dam iron oxide-copper-gold deposit is rarely preserved, but represents an early product of *in-situ* transformation of primary uraninite. Electron back-scatter diffraction data (Inverse Pole Figure, Image Quality and Grain Reference Orientation Deviation mapping) reveal formation of zoned uraninite to be the result of a sequence of superimposed effects rather than from primary growth mechanisms alone. This is the first known microstructural analysis of uraninite showing crystal-plastic deformation of uraninite via formation and migration of defects and dislocations into tilt boundaries. Defining grain-scale characteristics and microstructural features in radiogenically modified minerals like uraninite carries implications in better understanding the processes involved in their formation, highlights limitations in the use of uraninite for U-Pb chemical ages, as well as for constraining the incorporation and release of daughter radioisotopes, especially where zoning, porosity, fractures and microstructures are present.

Keywords: Uraninite, EBSD, chemical zoning, tilt boundaries, microstructures, Olympic Dam

INTRODUCTION

Compositional zoning is a common phenomenon in minerals (e.g., Shore and Fowler, 1996, and references therein). Such zoning has, however, only rarely been reported for uraninite (e.g., Alexandre et al., 2015; Macmillan et al., 2016) despite the frequently observed high concentrations of impurity

elements including: Ca, Pb, REE+Y (hereafter ΣREY), Th, Fe, Si, P, Al, Mg, Mn, K, and many others (e.g., Finch and Murakami, 1999). The ~1590 Ma Olympic Dam (OD) iron-oxide copper gold deposit is unusually rich in uranium where uraninite (ideally UO_2) is one of three main U-minerals (the others are coffinite and brannerite; Ehrig et al., 2012, and references therein). Two generations of uraninite, comprising four main textural classes are identified at OD (Macmillan et al., 2016): 1) 'primary', 2) 'zoned', 3) 'cob-web' and 4) 'massive'. Of relevance here are the 'early' generation (Classes 1-3), all characterized by Pb- and ΣREY-rich (up to 0.42 apfu collectively) single grains (tens to hundreds of μm in size). Differentiation between classes of 'early' uraninite is based on textural and chemical zonation patterns (Macmillan et al., 2016). The authors show that 'primary' uraninite represents the least-altered, most pristine, crystalline uraninite, whereas 'zoned' and 'cob-web' types have undergone chemical-textural modifications by *in-situ* alteration processes (i.e., single grains of 'primary' uraninite are progressively altered via solid-state diffusion followed by interaction with hydrothermal fluids to form 'zoned' through to 'cob-web' uraninite). The 'cob-web' class consists of rhythmic intergrowths of uraninite and sulfides from core to margin within any given grain. In contrast, changes in chemical zonation patterns relative to grain morphologies used to define 'zoned' uraninite as distinct from the 'primary' uraninite is less well constrained, and is the subject of the present study. The main question addressed here, is whether there is a link between the chemical zoning and microstructures within grains that show such modifications, and if so, could this provide clues in understanding the crystallization and alteration history of uraninite.

BACKGROUND AND RATIONALE

Morphological changes between internal zoning and the margin outline as seen in grains from the 'zoned' class of uraninite (Macmillan et al., 2016) can result either from primary crystallization processes, during which rates and growth orientation change (e.g., in garnet; Allen and Buseck 1988), or from dynamic recrystallization in a broad range of geological environments (e.g., Urai et al., 1986;

Steffen and Selverstone, 2006). The combined use of electron back-scatter diffraction (EBSD) and orientation contrast (OC) imaging to study microstructures within minerals can be applied to any mineral at a range of scales (Prior et al., 1999). From EBSD and OC data it is possible to quantify microstructures empirically and constrain dislocation slip systems, and this coupled with other micro- and nanoscale observations can lead to a more rigorous understanding of the formation of the observed mineral textures. The presence of microstructures, boundaries and interfaces (i.e., slip systems, sub-grain boundaries) have been shown to be important in controlling alteration processes, and the formation of micro- and meso-textures (Prior et al., 1999 and 2002).

The use of microstructural data from EBSD and OC imaging has been the subject of numerous studies to quantify the formation of various mineral textures. In zircon, microstructural features may form as a result of a combination of primary growth characteristics, degree of radiation damage, and recovery from crystal-plastic deformation, e.g., formation of dislocations, low-angle grain boundaries, and movement of slip systems (e.g., Reddy et al., 2006). In other minerals (e.g., garnet, spinel) there are strong crystallographic preferred orientations and these microstructural features are shown to be linked to slip systems, dislocation creep and recovery (Boyle et al., 1998; Prior et al., 2002).

Defining grain-scale characteristics in radiogenically modified minerals like zircon or uraninite is important for constraining their geologic evolution or U-Pb ages, particularly when zoning, porosity, fractures and microstructures are present. Incorporation and release of daughter products of ^{235}U and ^{238}U decay such as ^{207}Pb and ^{206}Pb, respectively, depend upon the robustness of the crystal lattice to radiation damage (i.e., amorphization and healing rates), as well as external factors such as exposure to hydrothermal fluids. In contrast to zircon, healing rates are considered much faster for uraninite and the mineral does not suffer from amorphization due to radiation damage (e.g., Janeczek and Ewing, 1991).

There are three slip systems identified for UO_2: $\{001\}\langle 1\bar{1}0\rangle$, at room temperature and atmospheric pressure, and $\{110\}\langle 1\bar{1}0\rangle$ or $\{111\}\langle 1\bar{1}0\rangle$, at higher temperatures (Kelly et al., 2012). Any of these

could be activated to generate microstructures during various processes, including concentration and/or release of minor/trace elements in uraninite. Here we employ EBSD analysis to study uraninite that has the necessary prerequisites to show relationships between minor element redistribution (modification of chemical zoning, fracture infill and mineral inclusions; Macmillan et al., 2016) and microstructures resulting from lattice distortion.

ANALYTICAL METHODOLOGY

Quantitative analysis of uraninite was performed using a Cameca SX-Five Electron Probe Micro-Analyzer (EPMA; Adelaide Microscopy, University of Adelaide) equipped with 5 tunable wavelength-dispersive spectrometers (WDS). Twenty-eight elements were measured; methodologies for data collection/analysis are given in Macmillan et al. (2016) and Appendix 1. The EPMA was also used to generate WDS elemental maps including those for Pb (Mα) and Ce (Lα) in Fig. 1a and b, respectively.

Electron back-scatter diffraction (EBSD) data were collected using the EDAX-TSL™ EBSD system on a FEI Helios NanoLab DualBeam™ FIB/SEM platform (Adelaide Microscopy). Analytical details are given in Appendix 1. Three data processing methods are applied: Inverse Pole Figure (IPF), Grain Reference Orientation Deviation (GROD) and Image Quality (IQ) mapping.

RESULTS

The uraninite studied is zoned with respect to minor elements, with Pb and ΣREY (Ce is a proxy for LREE) having the highest concentrations, and these co-correlate with one another (Fig. 1a and b). The presence of discrete REY-minerals as minute inclusions can also be inferred from the Ce map (Fig. 1b). This grain was chosen because the chemical patterns show two, (Pb+ΣREY)-poor, porous and fractured domains with equant-rhombic shape, aligned along the long axis of the planar section. One side of the section also displays edges parallel to the rhomb faces. Bornite and fluorite are also present as infill of fractures (Fig. 1a). Such a zonation pattern relative to the morphology of the grain, could indicate a type of sector zoning during primary growth, or alternatively, relate to secondary processes involving

minor element redistribution within the grain. Based on the color coding of the IPF map (Fig. 1c and d), the grain orientation lies between the $\langle 111 \rangle$, $\langle 001 \rangle$ and $\langle 101 \rangle$ zone axes, and has been estimated as $\langle 11\bar{2} \rangle$ (based on simulation of pole figures in Fig. A1, Appendix 2). Face indexing of the grain is shown accordingly on Fig. 1c.

The subtle gradational color variations on the IPF map (Fig. 1c and d) indicate gradual changes in crystallographic orientation but no apparent relationships with the chemical zoning. The boundaries formed by a lattice rotation about the plane normal to several directions have been superimposed on the IPF and IQ maps, as have low-angle grain boundaries on the GROD map (Figs. 1 to 3). This was appropriate to test if there was any relationship between these boundaries and the known slip systems for UO_2. Slip systems such as $\{111\}\langle 1\bar{1}0 \rangle$, with rotation about the $\langle 11\bar{2} \rangle$ direction, and which correspond to the present grain orientation, show only a few tilt boundary traces on the IPF map (Fig. 1c), indicating little correlation between microstructures and chemical heterogeneity in the grain. In contrast, superimposed tilt boundaries formed by lattice rotation about $\langle 1\bar{1}0 \rangle$, normal to $\{001\}\langle 1\bar{1}0 \rangle$, but different to the present grain orientation, correlate with bornite ± fluorite infilled cracks, arrays of inclusions, and some of the chemical zonation boundaries on the IPF map (Fig. 1d).

Intragranular orientation deviation as displayed by GROD mapping (Fig. 2a) occurs as a response to deformation, or where there is stored strain (relative to a reference orientation) within a grain. There are variations in intragrain crystallographic orientations of up to 18°, although the majority of the grain has an orientation of between 3.5° and 7° (green) compared to the reference (blue, marked by a white cross). Moreover, the misorientation profile (Fig. 2b) displays the range of orientations along the A-B profile delineated on the GROD map. Low-angle grain boundaries (<10°) are superimposed on the GROD map, and correlate with the tilt boundaries plotted on the IPF and IQ maps (Figs. 1d and 3a). Areas that appear to have higher relative stored strain (yellow-red) are found in regions that have a higher concentration of, or are surrounded by, many low-angle grain boundaries (Fig. 2a). When

comparison is made between the tilt boundaries circled (black dotted lines on Fig. 1d) and the compositional maps (Figs. 1a and b), the shape of the concentration boundaries of (Pb+ΣREY) appear similar to that of some of the tilt boundaries.

The IQ map (Fig. 3a) shows weak correlation with the chemical zonation pattern where zones of higher and lower IQ correlate with domains of elevated and lower (Pb+ΣREY), respectively. It is unclear whether observed variation in IQ is due to chemical variability alone, or to a combination of chemical variability and porosity/inclusion content, since the zones where IQ and chemical variability correlate also have higher porosity/inclusion content.

DISCUSSION

Primary versus secondary minor/trace element patterns

The continual production of Pb as a result of radioactive decay, will cause some alteration to the chemistry and structure of uraninite and/or any other U-bearing minerals (Hazen et al., 2009, and references therein). An important, self-induced alteration phenomenon which affects all U-bearing minerals is the accumulation of long-term damage caused by α-decay events, or 'metamictization'. The most intense damage results in defect production and amorphization as, for example, has been shown for modelling of energetic uranium recoil damage within zircon (Devanathan et al., 2006). In contrast, uraninite is known to be quite resistant to α-recoil events because of relatively rapid annealing kinetics (Eyal and Fleischer, 1985; Janeczek and Ewing, 1991), and has the ability to self-heal radiation damage; the radioactive decay process can also induce redistribution of key elements such as Pb within a given grain (e.g., Hazen et al., 2009).

Incorporation of Pb and ΣREY within the crystal lattice was shown for 'primary', oscillatory-zoned uraninite which hosts the highest amounts of Pb (up to 0.2 apfu) and ΣREY (up to 0.2 apfu) and thus was defined as the earliest uraninite generation at OD (Macmillan et al., 2016). Although oxidation of U^{4+} to U^{6+} was calculated to compensate for substitutions and charge balance, no changes to crystal

symmetry or lattice defects were found in such highly-substituted uraninite despite prediction of vacancies or other crystal structural modifications (Janeczek and Ewing, 1991). If all measured Pb is assumed as radiogenic, the oscillatory zoning with respect to Pb (and ΣREY) typical of primary uraninite at OD (Macmillan et al., 2016) is a self-induced diffusion patterning mechanism which traps daughter isotopes formed during α-recoil events. Weak oscillatory zoning with respect to (Pb+ΣREY) is also observed in the Th-U sector zoned uraninite from Mesoproterozoic pegmatite in Southern Norway, where the sector zoning is attributed to primary growth (Alexandre et al., 2015).

Zones of comparable low-(Pb+ΣREY) concentrations with those discussed here for the square-shaped-sectors (< 0.1 apfu for Pb and ~ 0.1 apfu for ΣREY) in the 'zoned' type were also reported, but only as incipient sectorial zoning on $\langle h0l \rangle$ or equivalent directions in the 'primary' uraninite from OD (Macmillan et al., 2016). Also documented by these authors, were the presence of rare, fine particles of galena in parts of 'primary' uraninite grains affected by sub-µm fractures, infilled with bornite ± fluorite. Zonation patterns (of Pb) which are oscillatory, sectorial, or a combination thereof, can be the result of element redistribution during the same or sequential self-induced α-recoil 'dry' events, and/or as a result of the interaction with fluids of differing chemistry (Cu, S, F) to uraninite. Bornite ± fluorite inclusions and infill, are more abundant in the 'zoned' uraninite, and these can be used to elucidate fluid chemistry. Microstructural analysis is essential in being able to link the observed chemical patterns and heterogeneity with micro- and meso-scale lattice defects that could have assisted ingress of fluids during superimposed geological events.

Lattice distortion and chemical heterogeneity

The microstructural analysis of 'zoned' uraninite shows lattice rotation/dislocations tied to preferential slip systems, low-angle boundaries and areas of high-strain. All these microstructures correlate with directions/traces of chemical heterogeneity in the grain, i.e., (Pb+ΣREY)-zonation, pores, inclusions and (bornite ± fluorite)-infilled cracks. The correlation between lattice rotation about the

$\langle 1\bar{1}0 \rangle$ direction on $\{001\}\langle 1\bar{1}0 \rangle$ slip system and the majority of tilt traces on the IPF map (Fig. 1d) indicates that accumulation of dislocations and pile-up defects are attributable to the low-temperature slip system in UO_2 (Boyle et al., 1998; Kelly et al., 2012). Such a system is active during superimposed alteration since it is controlled by directions different to the grain orientation.

Lattice distortion, coincident with directions parallel to {201} and {021} faces of sector zoning (indicated by dashed lines on Fig. 1d), and also with the orientation of infilled fractures, is highest in areas of high-stored strain accommodated by an increase in the abundance of low-angle boundaries (misorientation profile on the GROD map; Fig. 2). Therefore, fracturing of uraninite could be considered the result of strain hardening by dislocation pile-up along chemical boundaries that impede dislocation glide and prohibit recovery. This is plausible since there is a considerable amount of strain energy stored in the region around a dislocation (Kelly et al., 2012).

Any distortions to the crystal lattice within the diffracting volume are recorded by IQ, and can be used as a qualitative indicator of sample microstructure (e.g., variable crystallographic orientations; grain boundaries; chemical variability; impurities; porosity; Reddy et al., 2007). Correlation between chemical heterogeneity and sample microstructure is observed from the diffuse patterns recorded from the (Pb+ΣREY)-low, high-U sectors on the IQ maps (orange regions in Fig. 3). Such areas should display brighter patterns due to the higher atomic scattering effect produced by heavier elements (Wright and Nowell, 2006), but the presence of μm to sub- μm-scale inclusions/pores as dense fields instead induces diffuse diffraction patterns and thus lowers IQ.

All the above support the interpretation that the observed (Pb+ΣREY)-sector zoning is a result of the removal of these elements from pre-existing uraninite. Zones of structural weakness were formed as a result of the accumulation of defects and dislocations into tilt boundaries, which formed via lattice rotation about the plane normal to the active slip system in uraninite, permitting the ingress of a hydrothermal fluid into uraninite. Where dislocations and defects pile-up (i.e., along active slip

systems), high-diffusivity pathways can be formed, aiding element mobility (Reddy et al., 2006). Replacement of uraninite by bornite ± fluorite occurred along these planes, and these share common crystallographic orientations (both pink/orange in Fig. 1c and d). The same fluids are likely responsible for the presence of other trace elements, such as Ca and As within the (Pb+ΣREY)-depleted sectors (Macmillan et al., 2016), as well as increased pore/inclusion content. The documentation of low-angle boundaries associated with high strain areas provides evidence for a dynamic rather than a static recovery process. Thus the ability for uraninite to progressively self-anneal radiation damage (in contrast to static temperature-driven annealing processes) may have modified the chemical zoning, but more importantly, the interaction between uraninite and ingressing fluids must have been pivotal in forming the modified zonation patterns observed in 'zoned' uraninites.

The results here are further evidence that the 'zoned' uraninite is a distinct, intermediate stage during *in-situ* transformation of uraninite from 'primary' to 'cob-web' stages (Macmillan et al., 2016). In the last stage (Fig. A2, Appendix 2) pseudomorphic sulfide replacement of uraninite is more intense and leads to extremely modified forms of 'zoned' type, with the microstructural features (i.e., GROD, IQ maps) for 'cob-web' uraninite being a variant of those displayed for 'zoned' uraninite (Figs. 1 to 3).

IMPLICATIONS AND OUTLOOK

Uraninite at OD has been exposed to a prolonged geologic history and has undergone multiple fluid-rock interaction events at variable flow rates, fluid-pressures, temperatures and rheologic contexts since early stage deposit formation at ~1590 Ma (Ciobanu et al., 2013). The interpretation of the evolution of uraninite is important in constraining mineralizing stages at OD and elsewhere. Future U-Pb uraninite geochronology requires a detailed knowledge of the inherent heterogeneity within these uraninites, since these dating methods assume chemical homogeneity at the scale of the microprobe beam. Thus, without combined microchemical and microstructural studies such as this, characterization of the heterogeneity is not possible, and erroneous chemical ages may be attained. This type of work should

be applied to other U-bearing minerals featuring comparable chemical-textural complexity such as hematite (Ciobanu et al., 2013), an intrinsic hydrothermal mineral in IOCG deposits.

ACKNOWLEDGEMENTS

This work forms part of the Ph.D. studies of EM and is supported by BHP Billiton. NJC, KE and AP acknowledge support from the ARC Research Hub for Australian Copper-Uranium. Staff at Adelaide Microscopy are thanked for instrument training. We appreciate insightful comments and suggestions from reviewers Mark Pearce, Alan Boyle and Paul Alexandre, and Editor Ian Swainson, which assisted us with revision of the manuscript.

REFERENCES CITED

Alexandre, P., Peterson, R. and Joy, B. (2015) Sector zoning in uraninite. The Canadian Mineralogist, 53, 1-11.

Allen, F.M. and Buseck, P.R. (1988) XRD, FTIR, and TEM studies of optically anisotropic grossular garnet. American Mineralogist, 73, 568-584.

Boyle, A.P., Prior, D.J., Banham, M.H. and Timms, N.E. (1998) Plastic deformation of metamorphic pyrite: new evidence from electron backscatter diffraction and forescatter orientation contrast imaging. Mineralium Deposita, 34, 71-81.

Ciobanu, C.L., Wade, B.P., Cook, N.J., Schmidt Mumm, A. and Giles, D. (2013) Uranium-bearing hematite from the Olympic Dam Cu–U–Au deposit, South Australia: A geochemical tracer and reconnaissance Pb–Pb geochronometer. Precambrian Research, 238, 129-147.

Devanathan, R., Corrales, L.R., Weber, W.J., Chartier, A. and Meis, C. (2006) Molecular dynamics simulation of energetic uranium recoil damage in zircon. Molecular Simulation, 32, 1069-1077.

Ehrig, K., McPhie, J. and Kamenetsky, V. (2012) Geology and mineralogical zonation of the Olympic Dam Iron Oxide Cu-U-Au-Ag deposit, South Australia. Special Publication Number 16 - Geology and Genesis of Major Copper Deposits, Society of Economic Geologists, 237-267.

Eyal, Y. and Fleischer, R.L. (1985) Timescale of natural annealing in radioactive minerals affects retardation of radiation-damage-induced leaching. Nature, 314, 518-520.

Finch, R.J. and Murakami, T. (1999) Systematics and paragenesis of uranium minerals. In P.C. Burns and R.J.

Finch, Eds., Uranium: Mineralogy, Geochemistry and the Environment, 38, p. 91-179. Reviews in Mineralogy and Geochemistry, Mineralogical Society of America, Chantilly, Virginia.

Hazen, R.M., Ewing, R.C. and Sverjensky, D.A. (2009) Evolution of uranium and thorium minerals. American Mineralogist, 94, 1293-1311.

Janeczek, J. and Ewing, R.C. (1991) X-ray powder diffraction study of annealed uraninite. Journal of Nuclear Materials, 185, 66-77.

Kelly, A.A., Knowles, K.M. and Kelly, A. (2012) Crystallography and crystal defects. 2nd ed., John Wiley and Sons, Chichester, West Sussex, UK.

Macmillan, E., Cook, N.J., Ehrig, K., Ciobanu, C.L. and Pring, A. (2016) Uraninite from the Olympic Dam IOCG-U-Ag deposit: linking textural and compositional variation to temporal evolution. American Mineralogist, 101, 1295-1320.

Prior, D.J., Boyle, A.P., Brenker, F., Cheadle, M.C., Day, A., Lopez, G., Peruzzo, L., Potts, G.J., Reddy, S., Spiess, R., Timms, N.E., Trimby, P., Wheeler, J. and Zetterstrom, L. (1999) The application of electron backscatter diffraction and orientation contrast imaging in the SEM to textural problems in rocks. American Mineralogist, 84, 1741-1759.

Prior, D.J., Wheeler, J., Peruzzo, L., Spiess, R. and Storey, C. (2002) Some garnet microstructures: an illustration of the potential of orientation maps and misorientation analysis in microstructural studies. Journal of Structural Geology, 24, 999-1011.

Reddy, S.M., Timms, N.E., Trimby, P., Kinny, P.D., Buchan, C. and Blake, K. (2006) Crystal-plastic deformation of zircon: A defect in the assumption of chemical robustness. Geology, 34, 257-260.

Reddy, S.M., Timms, N.E., Pantleon, W. and Trimby, P. (2007) Quantitative characterization of plastic deformation of zircon and geological implications. Contributions to Mineralogy and Petrology, 153, 625-645.

Shore, M. and Fowler, A.D. (1996) Oscillatory zoning in minerals: a common phenomenon. Canadian Mineralogist, 34, 1111-1126.

Steffen, K.J. and Selverstone, J. (2006) Retrieval of P-T information from shear zones: thermobarometric consequences of changes in plagioclase deformation mechanisms. Contributions to Mineralogy and Petrology, 151, 600-614.

Urai, J.L., Means, W.D.M. and Lister, G.S. (1986) Dynamic recrystallisation of minerals. In B.E. Hobbs and H.C. Heard, Eds., Mineral and Rock Deformation: Laboratory Studies - The Paterson Volume, Geophysical Monograph 36, p. 161-199. American Geophysical Union.

Wright, S.I. and Nowell, M.M. (2006) EBSD image quality mapping. Microscopy and Microanalysis, 12, 72-84.

FIGURE CAPTIONS

Fig. 1: **(a, b)** EPMA-WDS maps showing Pb and Ce zonation in uraninite (Urn; adapted from Macmillan et al., 2016), with cracks infilled by bornite (Bn) and fluorite (Fl). Red-dotted lines demarcate (Pb+ΣREY)-poor sectors); **(c-d)** EBSD-derived $\langle 001 \rangle$ Inverse Pole Figure (IPF) map of UO_2 with superimposed tilt boundaries formed by a lattice rotation about the plane normal to $\{111\}\langle 1\bar{1}0 \rangle$ in (c) and $\{001\}\langle 1\bar{1}0 \rangle$ in (d). UO_2 is of one dominant orientation (close to $\langle 11\bar{2} \rangle$ zone axis) and represents a single grain with some gradational color variation reflecting slight distortion of crystal lattice. White- and black-dotted circled areas highlight two examples of where the tilt boundaries correlate to Ce zonation boundaries (Fig. 1b and d, respectively). Mean compositions (wt%) of low-Pb zones: 75.5 UO_2, 6.7 PbO_2, 3.4 CaO, 7.1 ΣREY_2O_3, 1.2 As_2O_3; high-Pb zones: 69.8 UO_2, 14.9 PbO_2, 1.6 CaO, 11.0 ΣREY_2O_3, 0.3 As_2O_3 (as reported in Macmillan et al., 2016).

Fig. 2 **(a)** EBSD-derived Grain Reference Orientation Deviation (GROD) map of UO_2 with superimposed <10° low-angle grain boundaries (solid black lines). Each pixel is colored from reference orientation (blue, defined by white cross) with misorientation of up to 18° (red). Misorientation profile (Fig. 2b) plotted along section A-B; **(b)** EBSD-derived misorientation profile displaying the highest misorientation (~9°) correlates to zones of higher strain (yellow on Fig. 2a).

Fig. 3: **(a)** EBSD-derived Image Quality (IQ) map of entire uraninite grain with superimposed tilt boundaries formed by a lattice rotation about the plane normal to $\{001\}\langle 1\bar{1}0 \rangle$. Warmer colors (red-orange) represent areas of higher IQ (uraninite), and cooler colors (blue-green) represent areas of lower IQ (bornite and fluorite). Orange colored areas (uraninite) represent low-Pb uraninite with higher inclusion content whereas red colored areas represent high-Pb uraninite with lower inclusion content. Black dotted circled regions are further enlarged in (c) and (d), and area outlined with black rectangle is imaged in (b); **(b)** BSE image of uraninite grain with reduced brightness and contrast to highlight increased Pb/ΣREY and reduced porosity towards rim (red dashed lines); **(c-d)** EBSD-derived Image Quality (IQ) maps of UO_2 (colored as for (a)). The uraninite regions with lower porosity and elevated Pb±ΣREY have higher IQ (red) than zones with lower porosity (orange).

This is a preprint, the final version is subject to change, of the American Mineralogist (MSA)
Cite as Authors (Year) Title. American Mineralogist, in press.
(DOI will not work until issue is live.) DOI: http://dx.doi.org/10.2138/am-2016-5753

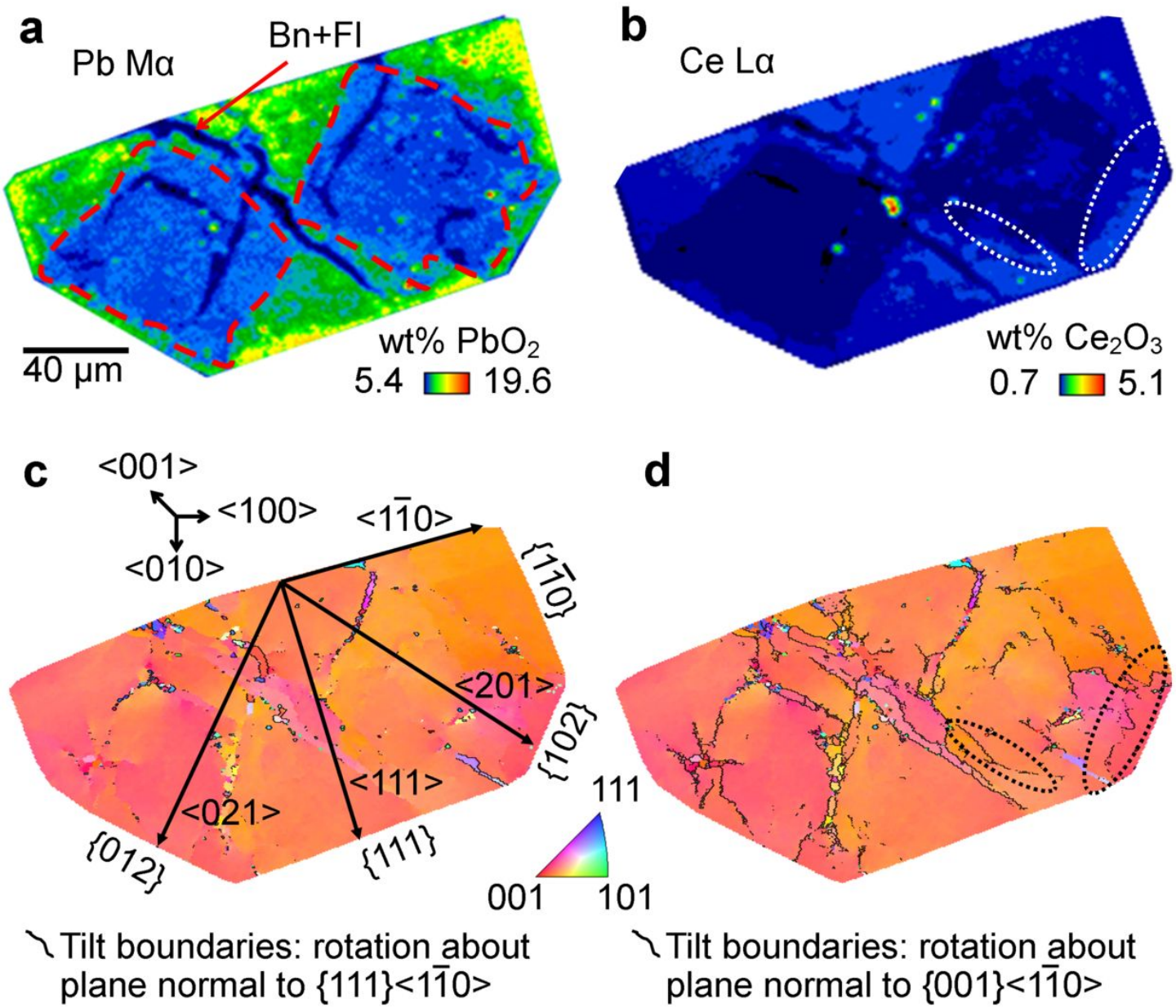

Figure 1 (Macmillan et al.)

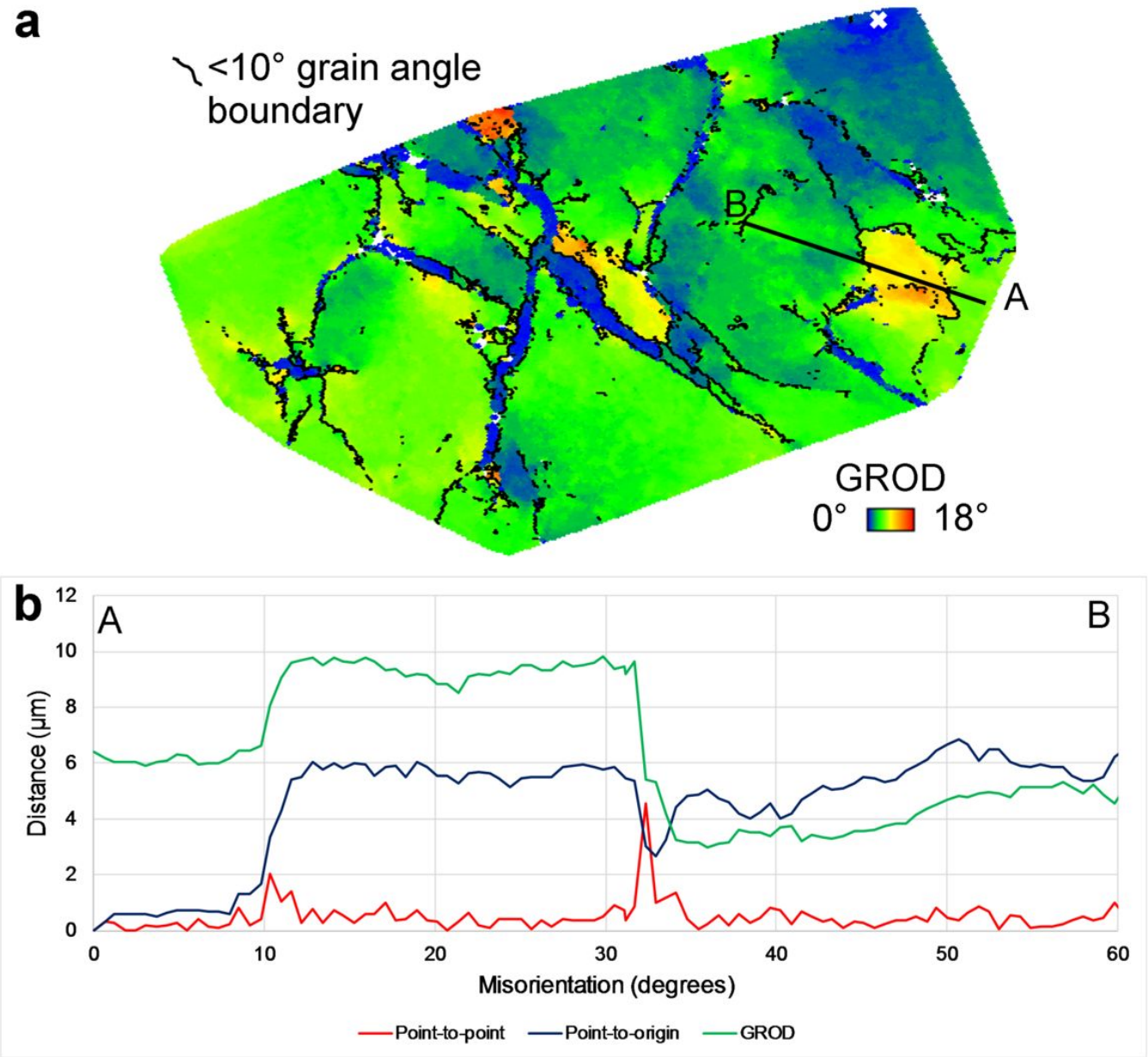

Figure 2 (Macmillan et al.)

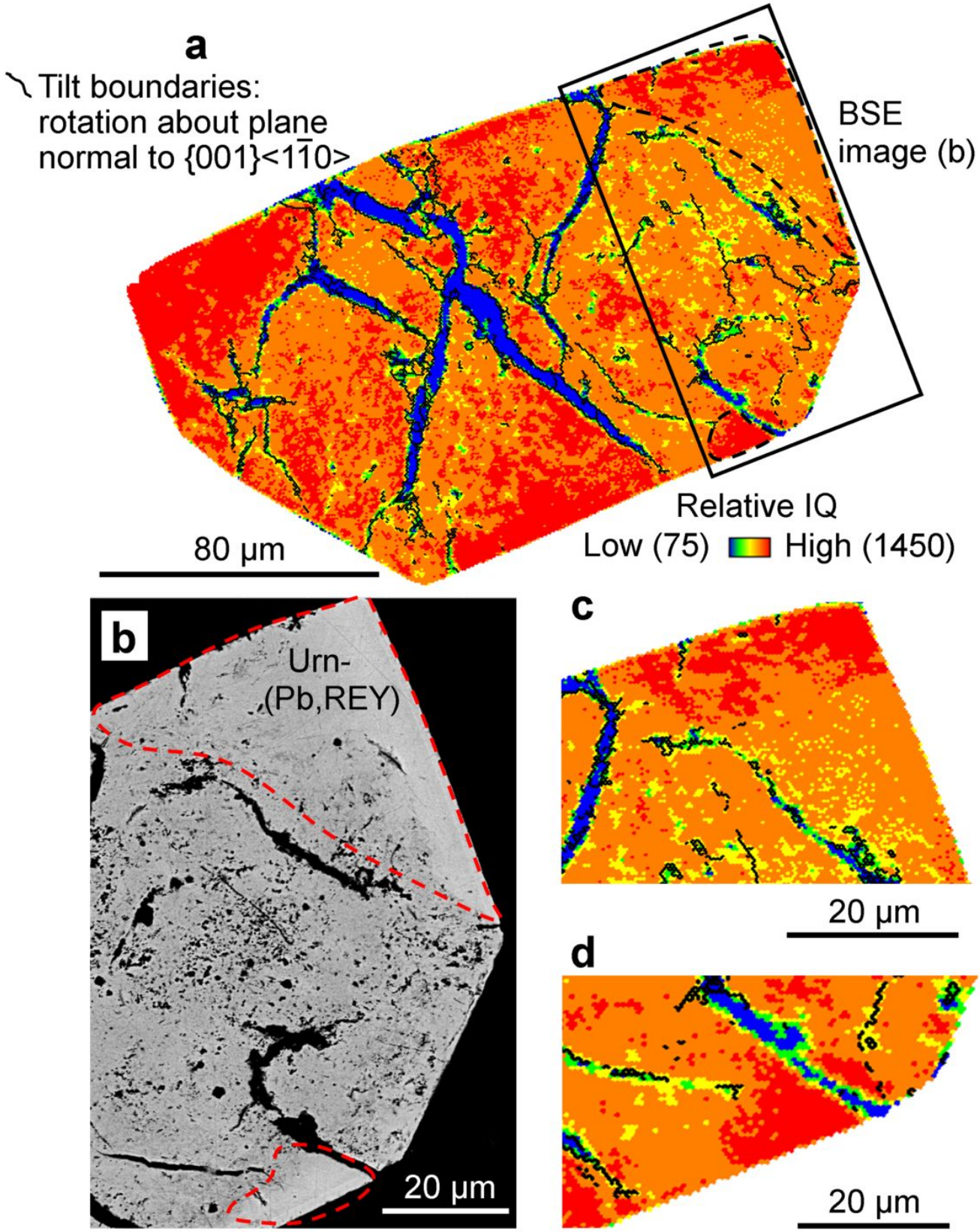

Figure 3 (Macmillan et al.)